

## On the nature of the EXor accretion events: an unfrequent manifestation of a common phenomenology ? <sup>1</sup>

D.Lorenzetti<sup>1</sup>, S.Antoniucci<sup>1</sup>, T.Giannini<sup>1</sup>, G.Li Causi<sup>1</sup>, P.Ventura<sup>1</sup>, A.A.Arkharov<sup>2</sup>, E.N.Kopatskaya<sup>3</sup>, V.M.Larionov<sup>2,3,4</sup>, A.Di Paola<sup>1</sup>, and B.Nisini<sup>1</sup>.

### ABSTRACT

We present the results of a comparison between classical and newly identified EXor based on literature data and aimed at recognizing possible differences or similarities of both categories. Optical and near-IR two-color diagrams, modalities of fluctuations, and derived values of the mass accretion rates are indicative of strong similarities between the two samples. We demonstrate how the difference between the outburst and the quiescence spectral energy distribution of all the EXor can be well fitted with a single blackbody, as if an additional thermal component appears during the outbursting phase. Temperatures of this additional component span between 1000 and 4500 K, while the radii of the emitting regions (assumed to be a uniform disk) span between 0.01 and 0.1 AU, sizes typical of the inner portions of the circumstellar disk. Spots persisting up to 50% of the outburst duration, not exceeding the 10% of the stellar surface, and with temperatures compatible with the EXor mass accretion rates, are able to account for both the appearance of the additional thermal component and the dust sublimation in the inner structures of the disk. We also compare the EXor events with the most significant color and magnitude fluctuations of active T Tauri stars finding that (i) burst accretion phenomena should also be important for this latter class; (ii) EXor events could be more frequent than those accidentally discovered. Remarkable is the case of the source V2493 Cyg, a T Tauri

---

<sup>1</sup>INAF - Osservatorio Astronomico di Roma, via Frascati 33, 00040 Monte Porzio, Italy, dario.lorenzetti, simone.antonucci, teresa.giannini, gianluca.licausi, andrea.dipaola, brunella.nisini, paolo.ventura@oa-roma.inaf.it

<sup>2</sup>Central Astronomical Observatory of Pulkovo, Pulkovskoe shosse 65, 196140 St.Petersburg, Russia, arkadi@arharov.ru

<sup>3</sup>Astronomical Institute of St.Petersburg University, Russia, vlar2@yandex.ru, enik1346@rambler.ru

<sup>4</sup>Isaac Newton Institute of Chile, St.Petersburg branch

star recently identified as a strong outbursting object: new optical and near-IR photometric and spectroscopic data are presented trying to clarify its EXor or FUor nature.

*Subject headings:* Stars: pre-main sequence – variable – emission lines – individual (V2493 Cyg) – Physical Data and Process: accretion disks – infrared: stars

## 1. Introduction

Young stellar objects (YSO's) from low to intermediate mass ( $0.5\text{-}8 M_{\odot}$ ), accumulate a large part of their final mass during the so-called main accretion phase (lasting about  $10^5$  yrs). After this period they continue to accrete, although at lower rates. The material repeatedly falls from the inner envelope onto their circumstellar disk, then crosses the viscous part of the disk itself and finally lands onto the star surface through the magnetic interconnection lines (Shu et al. 1994). This evolutionary stage is crucial for the comprehension of the star formation processes, because during this phase the accretion process halts, determining both the consequent evolution of the protostar and the Initial Mass Function (IMF) slope.

Disk accretion phenomena are characterized by intermittent outbursts (usually detected in the optical and near-IR bands) due to the sudden increase of the mass accretion rate (by orders of magnitude, Hartmann & Kenyon 1985). More recently, D'Angelo & Spruit (2010) presented a new work on the instability that can lead to episodic outbursts; they provided quantitative predictions for the episodic accretion on magnetized stars and indication that the cycle time of the bursts increases with a decreasing accretion rate. Such events are typical of many (if not all) YSO's. The outbursts of larger intensity ( $\gtrsim 4$  mag) are classified into two major classes: (*i*) EXor events (Herbig 1989) lasting one year or less, with a recurrence time of months to years, characterized by emission line spectra; (*ii*) FUor events (Hartmann & Kenyon 1985) of longer duration ( $\gtrsim$  tens of years) with spectra dominated by absorption lines.

However, it should be noted that an irregular photometric variability attributable to disk accretion is a defining feature of all the classical (i.e. most active) T Tauri stars (CTTS) and YSO's, although at lower levels of amplitude (typically 0.2-1 mag). Consequently, the

---

<sup>1</sup>Based on observations collected at AZT-24 telescope (Campo Imperatore, Italy), AZT-8 (Crimea, Ukraine), and LX-200 (St.Petersburg, Russia)

optical/near-IR intensity of most young stars tends to present random variations, and the EXor/FUor events could plausibly represent just extreme and incidentally observed cases of a widespread phenomenon.

Currently, doubts exist about the classification as EXor or FUor of some recently detected outbursts (see e.g. the case of V2493 Cyg - Miller et al 2011; Semkov & Peneva 2010; Kóspál et al. 2011). Sometimes even the origin of the observed variability is matter of debate (see e.g. the case of GM Cep - Sicilia-Aguilar et al. 2008; Xiao et al. 2010). These dubious circumstances arise from observations often relying on a single event and not on a long lasting photometric and/or spectroscopic monitoring. Remarkably, a single outburst does not allow us to ascertain if the object will remain or not in its higher state; analogously, from a single fading, we cannot decide whether we are looking at a typically bright object subjected to repetitive obscurations or, conversely, at a typically quiescent object that undergoes recurrent outbursts.

In the following, we will concentrate on the EXor class, whose typical phenomenology (outbursts, fading, recurrent activity) occurs on time-scales which are more easily accessible than those typical of FUor. So far, about 20 EXor systems are known which can be grouped into two sub-classes: the classical EXor (Herbig 1989, 2008), and the new identifications (see Sect.2 for the list of references). Hereafter, for simplicity, we will refer to these classes as classical and newest, respectively. Historically, the first group was identified in the visual band and, consequently, these accretion-disk systems are essentially unobscured (i.e. without significant envelopes). Later, the increasing availability of near-IR facilities quite naturally favored the identification of more embedded eruptive variables, typically associated with an optical-IR nebula (second sub-class). The membership to this latter class often relies on sporadic events and does not stem from a comprehensive analysis aimed at checking if the object presents all the properties typical of the classical prototypes (i.e. repetitive outbursts, rapid brightening and slower fading, colors pre-and post-outburst). In principle, there is no physical reason preventing the EXor phenomenon from occurring also during the more embedded (i.e. earlier) phase. In this scenario, the classical EXor, having already emerged from their dust cocoons, might be associated with later phases of the pre-main sequence evolution.

Here, to better clarify the EXor phenomenological framework we want: (*i*) to recognize possible similarities (or differences) between the two outbursting classes in terms of near-IR colors, shape of their spectral energy distribution (SED), and mass accretion rate; (*ii*) to compare the EXor variability with the more irregular one which is exhibited by a sample of CTTS observed in different epochs, searching for any common modality. In Sect.2 we present the investigated sample. Sect.3 and 4 are dedicated to analyze our sample and to compare

it with other CTTS, respectively. Our optical and near-IR monitoring of the outbursting source V2493 Cyg is commented in Sect.5. Concluding remarks are given in Sect.6.

## 2. The Sample

The sample is composed by the classical and newest EXor that are listed in the upper and lower part of Table 1, respectively. Here, the classical sources are identified with their commonly used names, while for some of the newest objects, the adopted names are those given in the General Catalogue of Variable Stars (GCVS - Kazarovets, Reipurth, & Samus (2011)). Indeed, different identification can be found in the recent literature: HA11 corresponds here to V1180 Cas, CTF93 216-2 to V2775 Ori, ISOChaI 192 to GM Cha, HBC 722 to V2493 Cyg, respectively. Each source is coded with an alphabetic letter (column 2), which will be used in the relevant figures. The range of the  $A_V$  parameter, as found in the literature, is given in column 5. The bolometric luminosity values (listed in column 6) refer sometimes to different parameters (photometric/accretion luminosity), opportunely indicated. In columns 7 and 8 a range of variability is given by listing the minimum and maximum V-band magnitude ever detected. Relevant references for the given parameters are provided in column 9.

The source PV Cep represents a fairly uncertain case: albeit included in the original Herbig's list, it is quite embedded, luminous, associated to an optical/near-IR nebula, therefore its nature is quite controversial (Kun et al. 2011a; Lorenzetti et al. 2011b). A comparative study of sample sources will also allow us to better ascertain the membership of the new entries.

## 3. Analysis and discussion

This Section will mainly deal with SED's and IR colors associated with different phases of both classical and newest EXor. It is worthwhile to anticipate that, as expected, much more extensive data exist for the newest sources. Indeed, their eruptive events have been sampled in a greater number of spectral bands (mainly IR) than the classical ones, whose light-curves were obtained from aperture photometry, typically performed in just one optical band (usually V or photographic). Due to observational constraints, this study has to rely on a still sparse and incomplete database. Nevertheless, the increasing number of monitoring efforts allows us to confirm (or not) the conclusions outlined here.

### 3.1. The near-IR two-colors diagram

For comparison purposes, in Figure 1 both the classical sources (depicted in blue) and the newest ones (in black) are displayed into the same two-colors plot  $[J-H],[H-K]$ . Magnitude values are taken from the literature data given in Table 3 and references therein. Source position is indicated by circles: the solid (open) circles indicate the color during the outburst (quiescent) state. The classical EXor (with the exception of PV Cep) are all located close to the locus of unobscured CTTS and present color variations that systematically deviate from the extinction law: passing from quiescence to outburst, they become substantially bluer, but show a  $[J-H]$  color that is larger than the one predicted on the basis of a pure extinction (Lorenzetti et al. 2007). Noticeably, the same behavior is shown also by the newest objects (with the possible exception of V1647 Ori and V2775 Ori), even if two main differences are recognizable with respect to the classical ones: (i) the newest objects occupy a redder portion of the plot and (ii) their color fluctuations are larger. The first occurrence is an obvious consequence of their location within more obscured regions (see the  $A_V$  values given in Table 1), as is often witnessed by the presence of an associated nebula; the second one comes from the fact that the light-curve of the newest sources was completely followed in the near-IR (thus providing the maximum range of color variations). No conclusion can be reached for LDN1415-IRS, and GM Cep, whose near-IR colors were obtained just once. Similar JHK diagrams, for smaller sub-samples of eruptive stars, are also given by Kóspál et al. (2011) and Kun et al. (2011b).

Summarizing, the majority of the newest objects present colors similar to those of classical ones, albeit extinguished by the expected (greater) amount.

### 3.2. The optical two-colors diagram

It is worthwhile to repeat the above analysis by using the optical colors from V, R, and I, (when available) for which extinction and scattering are both expected to play a major role (Figure 2). In analogy with the near-IR diagram, we indicate with blue (black) dots the points corresponding to the classical (newest) sources. For the reasons mentioned above, in the optical plot, the number of classical sources exceeds that of the newest ones. Two of these latter (SVS 13 and V1647 Ori, labelled as B and E, respectively) present color variations definitely not compatible with the predictions based on extinction, and the fluctuations exhibited by the classical cannot be accounted for with the  $A_V$  values derivable from the near-IR colors.

Summarizing, the color analysis confirms the well established fact that phenomena dif-

ferent from extinction have a significant role in determining EXor’s color variations. These latter, when derived by a single plot (VRI or JHK) could mimic an extinction variation which, however, is ruled out by the combined examination of both two-colors plots.

### 3.3. Accretion parameters

The comparison between classical and newest EXor can also benefit from the analysis of the mass accretion rate. This parameter can be derived by applying empirical relationships between the line luminosity and accretion luminosity (Antoniucci et al. 2011; Muzerolle et al. 1998). This latter can be translated into a mass accretion rate (Gullbring et al. 1998) under some assumptions on the stellar parameters and the inner disk radius. This method relies on intrinsic line fluxes, therefore the lack of an accurate estimate of the extinction allows to derive only approximated values for the accretion rate. The values available in the literature are collected in Table 2. Therein, the methods used for deriving  $\dot{M}_{acc}$  are mentioned, giving also reference to the original papers where the adopted assumptions are explained. In the same Table, the status of the source when the accretion rate was derived is coded as high (H), intermediate (I), or low (L).

Classical sources show  $\dot{M}_{acc}$  values in the interval  $0.6 \cdot 10^{-8}$  -  $2.4 \cdot 10^{-6}$   $M_{\odot}$   $\text{yr}^{-1}$ , whereas the newest ones  $1.6 \cdot 10^{-8}$  -  $1.8 \cdot 10^{-6}$   $M_{\odot}$   $\text{yr}^{-1}$ . Hence, among classes of objects having similar masses (FUor, EXor, T Tauri), EXor’s accretion rates appear comparable to T Tauri ones (typically  $10^{-7}$ ; Hartigan et al. 1995), but definitely lower than the typical rates of FUor objects ( $10^{-5}$ - $10^{-4}$ ; e.g. Hartmann & Kenyon 1985). Thus, no substantial difference is recognizable between the two classes, which appear once again very similar.

Data in Table 2, combined with what we know about the recurrence of EXor events, allow us to infer on the total mass the star is capable to accrete through these repetitive events. By assuming, quite conservatively, (*i*) a peak value of the accretion rate of  $2 \cdot 10^{-6}$   $M_{\odot}$   $\text{yr}^{-1}$ ; (*ii*) that passing from outburst to quiescence is equivalent to maintain a constant accretion equal to 50% of the peak value; (*iii*) that the outburst duration is 1/20 of the quiescent stage; (*iv*) and finally, that the total evolutionary time of the EXor phase is  $\leq 10^6$  yrs, then the total mass accreted during such phase is  $M = 2 \cdot 10^{-6} M_{\odot} \text{ yr}^{-1} \times 0.5 \times 0.05 \times (<10^6)\text{yrs} \leq 0.05 M_{\odot}$ , at maximum. Since Muzerolle et al. (1998) and Calvet et al. (2000) have already demonstrated that the steady disk accretion rate cannot be responsible for a significant fraction of the final stellar mass, the FUor mechanism remains the sole alternative to accrete a substantial mass via disk accretion. However, at the largest possible rate of  $10^{-4} M_{\odot} \text{ yr}^{-1}$ , 10 or 100 FUor bursts, each lasting  $10^3$  or  $10^2$  yrs, respectively, are required. These prescriptions appear fairly extreme and they confirm that the final stellar

mass is not quantitatively influenced by disk accretion during PMS.

### 3.4. The outburst Spectral Energy Distribution

Modeling the EXor SED’s is a subject afforded and discussed in a number of dedicated papers dealing with both individual sources (see references in Table 1) and the entire class of objects (mainly classical, see eg. Herbig 2008). Typically, these models refer to peculiar phases (outbursts or quiescence) or tend to interpret the overall observed phenomenology. Here we aim at comparing the SED corresponding to high and low states assumed coincident with, or close to, the outburst and quiescent phase, respectively. Our aim is twofold: *(i)* to understand if different outburst events can be taken back to a same observational phenomenology; *(ii)* if so, to investigate how the derivable parameters can be used to infer on a possible common mechanism. This scope looks quite ambitious, given the limits imposed by the scanty observational material available so far, but a first effort in that direction could be helpful for stimulating further investigations.

Aiming at reducing the number of approximations and assumptions, we have compared the SED’s only at those wavelengths where higher and lower state are both determined, so as to avoid any interpolation at wavelengths where only one SED is given. Such an approach forced us to use less photometric determinations than available, but assure us a more secure definition of the SED difference. The fluxes we used for classical and newest EXor are given in Table 3. These values are based on minor assumptions: *(i)* the photometric bands have been *standardized*, in the sense that they have been associated with a single wavelength, given in the Table notes, although the original fluxes were not necessarily obtained with the same bandpass; *(ii)* the photometric errors adopted in the fitting procedure are those given in the individual papers, otherwise, an uncertainty of 10% is assumed.

We started our analysis by checking whether the SED variation between high and low state can be described through a simple change of the amount of extinction. In this scenario an intervening mass, which normally obscures the emitting system during quiescence, should be recurrently removed during the outburst events. If this were true, the SED’s ratio should resemble an extinction curve. Adopting the extinction law by Rieke & Lebofsky (1985), we would obtain:

$$\frac{SED^{out}(\lambda)}{SED^{quies}(\lambda)} = 10^{-0.4\Delta A_\lambda} \quad (1)$$

where:  $\Delta A_\lambda = A_\lambda^{outburst} - A_\lambda^{quiescence}$ , with  $A_\lambda = A_V \left(\frac{5500}{\lambda}\right)^{1.75}$ .

However, we find that it is impossible to fit the photometric observations with the previous function for any sources of our sample. This confirms the result of section 3.1, i.e. that the observed photometric variations must be ascribed to an intrinsic phenomenology more than to a simple extinction change.

Hence, we explored the hypothesis that an additional thermal component appears during the outbursting phase, still allowing for a possible extinction variation between the quiescent and outburst stages. In more detail, for each source we fitted the difference of the two dereddened SED's (each corrected by the corresponding  $A_V$  at outburst or quiescence) with a pure blackbody function (BB):

$$\frac{SED^{out}(\lambda)}{10^{-0.4(A_\lambda + \Delta A_\lambda)}} - \frac{SED^{quies}(\lambda)}{10^{-0.4A_\lambda}} = \lambda \cdot BB(\lambda, T, R) \quad (2)$$

where each SED is given as  $\lambda F_\lambda$ ,  $A_\lambda$  is the extinction at quiescence,  $R$  is the radius of the emitting region (assumed to be a uniform disk), and  $T$  is its BB temperature. The free parameters are  $T$ ,  $R$ ,  $A_V$ , and  $\Delta A_V$ . We checked *a posteriori* that the derived  $A_V$ , and  $\Delta A_V$  values are roughly comparable with those given in the literature (see Table 1). This is not the case of two sources: V1647 Ori, and PV Cep, whose nature has been already considered quite uncertain (see Sect.2). We point out that the shape of the true emitting area (that we do not model) is likely very different from the assumed uniform disk: for example it could be the inner wall of the circumstellar disk; nevertheless the radius  $R$ , derived by the fit, still provides an indication of the length scale of the emission region.

Our results are depicted in Figure 3 and provide the indication that the appearance of a thermal component is a good representation of the observed phenomenon. Almost all the sources present a definite single temperature component spanning between 1000 K and 4500 K. Two exception can be noted: (i) EX Lup shows a higher temperature ( $\sim 20000$  K) BB coming from a very compact region (fraction of stellar radius): this result is not consistent with the value of 6500 K by Juhász et al. (2011) and this discrepancy will be discussed below; (ii) V2492, whose excess emission is barely fitted with a single BB (see also Kóspál et al. 2011). The temperature we derive for V1647 Ori is not conflicting with those by McGehee et al. (2004) and Walter et al. (2004), since here we are dealing with an excess temperature component instead of the  $T$  value at outburst. Minor corrections to the pure BB could be applied by accounting for the excess continuum emission observed in T Tauri through the IYJ bands (Fischer et al. 2011), but the existence of multiple contributions at substantially different temperatures seems to be ruled out. The output parameters of our fits are given in Table 4. As can be seen in our  $\chi^2$  maps (see Figure 4 and discussion below), there exists a range of temperatures  $T$  and radii  $R$  providing fits with a comparable  $\chi^2$  value. These ranges

are given in Table 4 for each source. Noticeably, such  $R$  values are smaller than the typical radius of the inner portion of accretion disks (Muzerolle et al. 2003), but this is expected, since we are assuming that the emission is ideally coming from a face-on disk centered on the star. Moreover, in Table 4 we see that the extinction variations  $\Delta A_V$  always present small negative values, the average value being  $-3.1 \pm 1.8$ , which means that the outburst tends not only to heat, but also to remove and sublimate some dust (see below). The large spread of temperature values likely reflects the large variety of morphological and physical conditions (inner disk size, opacity, density) more than being suggestive of a random sampling of a dynamical process at different epochs (e.g. the heating or cooling of a circumstellar region). To test this hypothesis, we applied our fit method also to SED's relative to intermediate epochs of the two sources (V1118 Ori and V1647 Ori) whose outburst periods are well covered by several optical/near-IR observations. If we looked at a progressive phenomenon, we should obtain temperatures increasing or decreasing with fluxes. Conversely, we obtain the same value of the temperature by fitting consecutive SED's which are not substantially far in time from the outburst. However, as time goes on, a single BB appears more and more inadequate to account for the data. This likely means that the existence of a single BB is well representative of the outburst, while a stratification of temperatures is more suitable to describe the intermediate phase toward the quiescence.

We tried to interpret this observational scenario by considering that the EXor accretion event leads to the onset of a hot spot on the stellar surface. The spot both warms the circumstellar region, whose thermal emission we are observing, and also contributes to dust sublimation. We rely on energy conservation by assuming that the energy irradiated by the spot equals the sum of that emitted by the surrounding region and that spent for dust sublimation. In practice, adopting an efficiency equal to unity, the spot power (i.e. luminosity) integrated for the spot duration should be equal to the total energy emitted during all the outburst by the inner disk (heated by the spot itself) plus the energy needed for sublimation.

An estimate of this latter can be obtained for a typical T Tauri star ( $M=0.5 M_\odot$ ,  $R=2 R_\odot$ ,  $T=4000\text{K}$ ). The sudden increase of  $\dot{M}_{acc}$  from 0.02 to  $6 \cdot 10^{-7}$  (assuming as typical the values of EX Lup - see Table 2) causes the accretion luminosity to increase from 0.05 to  $1.58 L_\odot$ . The dust inner disk which is located at about  $R_1=17 R_\odot$  in quiescence, increases up to  $R_2=30 R_\odot$  during the outburst (Muzerolle et al. 2003): obviously, the burst heats the inner zone and, consequently, moves the dusty disk away. We can find an upper limit of the energy spent for dust sublimation by assuming: (i) the dust is contained in the entire volume between  $R_1$  and  $R_2$ ; (ii) such dust evaporates completely. More precisely the sublimating dust is located within a cylinder having a radial width  $R_2-R_1$  and scale height ( $H$ ) related to the vertical density variation from the disk plane. Following Muzerolle et al. (2004), such volume ( $V$ ) and the internal gas mass ( $m$ ) are given by:

$$V = 4\pi(R_2^2 - R_1^2) \cdot H \qquad m = \rho \cdot V \qquad (3)$$

where:  $H=c_s/\omega$  is the height scale,  $c_s$  is the sound speed (given by  $c_s^2=KT/\mu m_H$ ),  $\omega$  is the keplerian velocity  $\omega^2 = GM/R_1$ , and  $\rho$  is the volume density of the inner disk, that can be obtained in terms of the surface density  $\sigma$  and the height scale  $H$ , as  $\rho = \sigma/2\pi H$ . With the numerical values for  $T$ ,  $R_1$ , and  $M$  given above, we obtain  $m = 5 \cdot 10^{27}$  g, which represents a large upper limit since neither the density decreasing from  $R_1$  and  $R_2$ , nor its vertical decreasing have been accounted for. Now, assuming a solar chemistry, half of the silicon locked onto olivine grains (olivine is the most stable silicate, see Gail & Sedlmayr 1999), and adopting the compilation of Sharp & Huebner (1990, their Table 2) to obtain the energy absorbed for the sublimation, we find that the total energy needed to sublimate the dust present in the inner disk is  $6.4 \cdot 10^{35}$  erg. Such amount of energy is released away in a very short time (minutes) and only a tiny fraction hits the inner disk, therefore it can be neglected in the energy budget.

The evaluation of the spot emission is done following the model by Calvet & Gullbring (1998) which predicts spot temperatures ( $T_{spot}$ ) between 6000 and 12000 K for different combination of stellar mass and radius and for a given accretion rate in the range of  $10^{-9}$ - $10^{-7}$   $M_\odot$  yr $^{-1}$ . The spot temperature roughly scales as  $(\dot{M}_{acc})^{1/4}$ , hence the EXor events, whose mass accretion rates span between  $2 \cdot 10^{-7}$  and  $2 \cdot 10^{-6}$   $M_\odot$  yr $^{-1}$  (see Table 2), should create spots with temperatures between 10000 and 18000 K, for typical values of stellar mass and radius ( $0.5 M_\odot$ ,  $2 R_\odot$ , respectively). Such spot temperatures give a barely detectable emission in the optical near-IR bands, which is not easily recognizable in the SED's difference.

The power emitted by the spot linearly depends on two factors: the time interval  $\tau$  during which the spot temperature remains at its maximum value (10000-18000K), expressed as a fraction of the outburst duration, and the spot surface  $\Sigma_{spot}$ , expressed as a fraction of the stellar surface. Given such linearity, we treated the product  $\tau \cdot \Sigma_{spot}$  as a single variable. For the given range of spot temperatures (from 10000 to 18000 K), two extreme values of the product  $\tau \cdot \Sigma_{spot}$  are indicated in blue and green in Figure 4, corresponding to 0.001 ( $\tau = 0.1 \times \Sigma_{spot} = 0.01$ ) and 0.05 ( $\tau = 0.5 \times \Sigma_{spot} = 0.1$ ), respectively. The considered upper value for  $\tau$  is compatible with the typical light curve (see e.g. V1118 Ori - Audard et al 2010) where the maximum flux level lasts about half of the total outburst duration. The lower value for  $\Sigma_{spot}$  are compatible with the sizes predicted by Calvet & Gullbring (1998).

In Figure 4, the area of intersection between the  $\chi^2$  minima and model predictions represent the T and R ranges for which the spot model can account for the observations. The derived ranges of T and R are depicted in Figure 4 as confidence contours (in yellow-orange) superposed on the  $\chi^2$  maps and are listed in Table 4.

Summarizing, for 8 out of the 10 investigated objects we find a BB fit in very good agreement with model predictions. Two extreme cases are EX Lup, which can be interpreted as a direct detection of hot spot emission, and PV Cep, whose observations are compatible with a marginal value of the emitting region radius ( $R = 0.2$  AU).

Hence, the increase of luminosity during the EXor event appears compatible with emission from an inner disk heated by a hot spot. It is worthwhile noting that Calvet & Gullbring (1998) model predicts an additional contribution to the heating (of about 30%) due to the column above the accretion shock (i.e. the pre-shock region): here, we assume it compensates possible efficiency losses currently ignored. This quantitative analysis of EXor events provides further support to the magnetospheric accretion infall model.

#### 4. Comparison with CTTSs

The second aim of our work is to search for similarities (or differences) between the photometric behaviour of the known EXor and those of randomly variable CTTSs. To perform a statistically significant comparison, we have searched the literature data for a large sample of sources for which there exist two photometric measurements, taken almost simultaneously in two different epochs. We selected the sample investigated by Cohen & Kuhl (1979) (hereafter CoKu), who observed through near-IR photometry and optical spectroscopy a large number of low-mass PMS sources belonging to different clouds. Twenty years later, during the 2MASS survey, practically all these sources were re-observed in the same bands. Data from both these surveys offer the chance of analyzing the modalities of the occurred variations (H, K bands) for 134 objects on a time-scale that, although not adequate to infer on the rising and declining duration of possible outburst events, is still suitable for a statistical investigation. Aiming at recognizing objects characterized by irregular variability, typically associated with eruptive events, we have excluded the sources potentially associated with periodic variations. Following the robust results by Herbst et al.(1994), we have excluded WTTSs (characterized by  $W_{H\alpha} < 10\text{\AA}$ ) mainly exhibiting cool spots, and we have considered only CTTSs (SpT. later than K0 and  $W_{H\alpha} > 10\text{\AA}$ ). Our final sample is composed by 120 objects, whose color variation as a function of the H magnitude variation is depicted in Figure 5.

We note that CoKu and 2MASS photometry were obtained with similar H-band filters ( $\lambda_{eff} = 1.65$  and  $1.66 \mu\text{m}$  for CoKu and 2MASS, respectively), but with different K-band filters ( $\lambda_{eff} = 2.31$  and  $2.16 \mu\text{m}$  for CoKu and 2MASS, respectively). This does not affect the difference between the two H magnitudes, but introduces systematic effects in the [H-K] color differences. We did not attempt to perform a color correction, which would be based

on *ad hoc* assumptions; instead, we take as (0,0) point the barycenter of the data distribution. Indeed, by looking at the Figure 5, we can see that the abscissa origin *indicated* by the data-point distribution (vertical green line) is practically identical to the nominal origin (dashed vertical line), while the same is not true for the ordinate axis, where a difference of about 0.1 mag is recognizable.

We identify with black dots all the 120 sources and with red circled those presenting variations above  $5\sigma$  in  $[\Delta H]$  and  $2.5\sigma$  in  $[\Delta(H-K)]$ . Correspondingly, black and red ellipses indicate the  $1\sigma$  distribution of the two groups. From the inspection of Figure 5 we can draw, although qualitatively, some noticeable statements: while the black ellipse does not show any peculiar orientation, the red one has its major axis definitely oriented toward the 1st and 3rd quadrants, that is those populated by sources that become bluer when brightening and redder when fading. The same behaviour is exhibited by EXor events (Lorenzetti et al. 2009 and references therein): therefore, in the framework of the PMS evolution, disk accretion phenomena, like those responsible for EXor bursts, seem to have a role also in accounting for the more frequent and less strong photometric variations typical of all CTTSs.

According to the above picture, EXor could represent rarer cases of a very common and widespread phenomenology displayed by all the CTTSs. This view is also supported by the accretion model recently presented by D’Angelo & Spruit (2010), who suggest the existence of a common mechanism that regulates both CTTS and EXor accretion events. Indeed, their predictions are able to explain both the strongest (EXor) and the weakest (CTTS) episodes of accretion, which would be determined by the interplay between the amount of gas that piles up in the inner region of the disk and the radius at which the keplerian frequency in the disk equals the star rotational frequency. The cyclic accretion solutions continue to exist indefinitely, also when the accretion rate decreases.

As a second output of our analysis, here we provide the identification of the sources that in Figure 5 display the largest photometric (and color) variations since, for that reason, they could be targeted in forthcoming observational programs. They all presented fluctuations  $\Delta H \simeq 1$  mag (or more) as V2493 Cyg (see next Sect.), and, noticeably, three of them, LkH $\alpha$ 154, LkH $\alpha$ 175 and LkH $\alpha$ 186 belong to the same cloud NGC7000/IC5070, while other three (NX Mon, LR Mon, and OY Mon) are located in NGC 2264. The circumstance that the most active CTTS cluster within only two well defined groups could be not fortuitous, but signals a larger frequency of accreting bursts in objects of the younger regions. In particular, NGC2264 (NGC7000) variables lie within 16 (65) arcmin, which corresponds to 0.06 (0.17) pc; the mutual closeness of these objects supports their covality and, in turn, the possibility that they are suitable EXor candidate, if such a phase were typical of the early evolution of any CTTS.

Several (complete) samples of T Tauri stars have been recently monitored at IR frequencies (e.g. YSOVAR, Morales-Calderón et al. 2011; PAIRTEL, Bloom et al. 2006; the surveys by Carpenter et al. 2001; Giannini et al. 2009; Alves de Oliveira et al. 2008) all aiming at establishing some statistics on the most relevant types of variability: i.e. rotational modulation by cool or hot spots, obscuration by dust, eruptive accretion. Strongly eruptive EXor are rare, but the identification of a couple of such objects (V2493 Cyg and V2492 Cyg) was provided by the mentioned surveys, which therefore could be effectively mined to determine plausible candidates.

## 5. The case of V2493 Cyg

Almost all the known EXor present frequent and smaller outbursts between two major events (see e.g. the behaviour of prototype EX Lup between the 1955 and 2008 outbursts - Aspin et al. 2010). Moreover, some EXor events might have occurred during the periods of weaker activity (of V2493 Cyg, but also of any other CTTS), but they might have been undetected because of the lack of a systematic monitoring. This latter consideration suggests that EXor events could be much more frequent than suggested by the few cases accidentally observed. An illustrative case is represented by the source indicated with an arrow in Figure 5. This is V2493 Cyg (*alias* LkH $\alpha$ 188G4), classified as CTTS until the summer 2010, and now recognized as an EXor object (Kóspál et al. 2011), or, possibly, as a FUor candidate mainly because of the presence of absorption lines in its optical and near-IR spectrum (Semkov & Peneva 2010, Miller et al 2011). The fact that V2493 Cyg was a CTTS undergoing smaller photometric variations (typically 1-2 mag) was obviously known since the 2MASS epoch.

What happened to V2493 Cyg (and to other observed CTTSs in outburst) could lead to the speculative conclusion that all CTTSs undergo an EXor phase. This latter could take place in the early CTTS lifetime, when the accretion rate is expectedly higher, or it could randomly appear during the subsequent evolution: the model of D’Angelo & Spruit tends to support the former hypothesis. Surely, given the scarcity of the observed cases, the EXor phase should be a short-lasting period of the PMS evolution.

Given the considerable interest provoked by its recent outburst discovery, we included V2493 Cyg among the targets of our EXor variables monitoring program. Our observations partially cover a period of about one year after the 2010 August outburst. Optical photometric (and very few polarimetric) observations were obtained with two nearly-identical photometers-polarimeters of the Astronomical Institute of St.Petersburg University, mounted on the 70cm AZT-8 telescope of the Crimean Observatory (Ukraine) and 40cm LX-200 tele-

scope of St.Petersburg University, respectively. Near-IR photometry and spectroscopy were obtained at the 1.1m AZT-24 telescope located at Campo Imperatore (L’Aquila - Italy). The exploited instrumentation along with the procedures for data acquisition and reduction are extensively described in Lorenzetti et al. (2006). Noticeably, the intra-day or day time-scale variations are not relevant for the discussion, so that observations in different bands not strictly simultaneous have been associated to the same date (within a maximum distance of 1 day). Photometric data are given in Table 5: they do not stem from a systematic monitoring. Our earliest observation is the first one of V2493 Cyg in outburst (Leoni et al. 2010), then a slow fading phase started, even if the quiescence pre-outburst state (corresponding to about 12 mag in H band) has never been reached.

Optical and near-IR data are presented in Table 5 and depicted as light-curves in Figure 6. These latter indicate that the source, after an early declining more pronounced in optical ( $\lesssim 1$  mag) than in near-IR bands ( $\approx 0.5$  mag), is in a steady state since about ten months. Some near-IR (I to K band) spectra of V2493 Cyg have been also taken during the monitoring period: given the limits imposed by our instrumentation, they appear quite noisy, however the systematic trend to become redder and redder while fading is recognizable. Moreover, two spectral features present in more than one spectrum can be identified (at a significant S/N level): the Pa $\beta$  HI at  $1.282\mu\text{m}$  and the CO band ( $2\rightarrow 0$ ) around  $2.35\mu\text{m}$ ; remarkably, they both appear always in absorption (see also Miller et al 2011). The persistence of a high flux level after the outburst and the presence of absorption features are defining properties of FUor objects more than of EXor, which tend to go back to their quiescent state within a short time (about 1 year) and usually present emission line spectra. Hence the possibility that V2493 Cyg underwent a FUor event cannot be ruled out, although the outburst mass accretion rate (see Table 2) is significantly lower than that found in FUor systems. Finally, we acquired several I band polarimetric measurements of this source, finding that it is remarkably stable at the level of 3-4%; the derived position angle has always the same value of  $158^\circ \pm 2^\circ$ , which should correspond to the disk orientation. The rather low polarization value is typical of a system viewed pole-on, or, in any case, of a system whose phenomenology is not disk-dominated, as in FU Ori events. Indeed, in this case, a small fraction of the light from the star is attenuated and the scattered/polarized light is typically low. In conclusion, to ascertain its real nature, V2493 Cyg certainly deserves a further monitoring during, at least, the next two years.

## 6. Concluding remarks

We have performed a systematical analysis based on literature data of both classical and newest identified EXor, mainly aiming at revealing similarities or differences between the two categories. In particular, we concentrated on optical/near-IR photometric data relative to two specific phases: outburst or quiescence. By comparing the SED's of both phases we infer on a possible mechanism responsible for the outburst itself. Based on our analysis, the following results can be summarized:

1. In the [J-H],[H-K] two-color diagram the newest sources appear indistinguishable with respect to the classical ones, suggesting that no intrinsic differences exists between the two categories. Only minor differences can be noted, due both to the embedness of the newest sources located in more extincted regions, and to a more complete observational sampling.
2. Optical [V-R],[R-I] and near-IR colors confirm that phenomena different from extinction may be significant in explaining the color variation associable with EXor outbursts (both classical and new).
3. The mass accretion rate ( $\dot{M}_{acc}$ ) exhibited by classical EXor span a slightly wider range with respect to the newest objects (0.006-2.4 vs. 0.016-1.8  $10^{-6} M_{\odot} \text{ yr}^{-1}$ ), but no substantial difference is recognizable between the two classes, which appear once again very similar. They both present  $\dot{M}_{acc}$  values that are comparable with the classical T Tauri ones and never reach the rates typical of FUor objects ( $10^{-5}$ - $10^{-4}$ ). When outbursting, EXor objects tend to have accretion rates an order of magnitude greater than in quiescence.
4. We computed the difference between the SED at high and low state (close to outburst and quiescence, respectively) for both classical and newest sources. All these differences are well fitted with a single blackbody whose temperature spans in the range 1000-4500 K, while the radii of the emitting regions span between 0.01 and 0.1 AU.
5. By adopting the hot spot model by Calvet & Gullbring (1998), the appearance of an additional blackbody during the outburst (up to few hundreds of days) can be interpreted in terms of heating of the inner parts of the accretion disk by a hot spot of 10000-18000 K having a size not exceeding 10% of the stellar surface.
7. A comparison with a large sample of active T Tauri stars shows that the most significant variations (both in magnitude and color) of these latter present the same modalities of EXor variations, although to a lesser extent. Hence, accretion phenomena have a dominating role also in the complex scenario of the CTTS variability.

8. This comparison leads us to speculate that EXor events might represent an infrequent manifestation of a rather common phenomenology displayed by all CTTSs. In this context, the rarity of EXor objects could be just due to the lack of a systematic monitoring.
9. In particular, one of the considered CTTSs, namely V2493 Cyg, underwent a strong accretion event in 2010 August, whose EXor or FUor nature is still controversial. Given the interest on this source, it was included in our list of monitoring program. Optical and near-IR observations (obtained in the period 2010-2011) have been presented. Basing on these preliminary data, its FUor nature cannot be ruled out, although a longer-lasting monitoring (at least a further couple of years) is needed for ascertaining its real nature.

## 7. Acknowledgements

We would like to thank the anonymous referee who significantly contributed to improve the present paper. We also thank Mauro Centrone and Riccardo Leoni for their support to the Campo Imperatore observing runs.

## REFERENCES

- Ábrahám, P., Kóspál, Á., Csizmadia, Sz., Moór, A., Kun, M., & Strigfellow, G. 2004, *A&A*, 419, L39
- Alves de Oliveira, C., & Casali, M. 2008, *A&A*, 485, 155A
- Andrews, S.M., Rothberg, B., & Simon, T. 2004, *ApJ*, 610, L45
- Antonucci, S. et al. 2011, *A&A*, 534A, 32A
- Aspin, C. 2011, *AJ*, 141:196
- Aspin, C., Beck, T.L., & Reipurth, B. 2008, *AJ*, 135, 423
- Aspin, C., & Reipurth, B. 2009, *AJ*, 138, 1137A
- Aspin, C., Reipurth, B., Herczeg, G.J., & Capak, P. 2010, *ApJ Lett.*, 719, L50
- Audard, M., Stringfellow, G.S., Güdel, M. et al. 2010 *A&A* 511, 63
- Back, T.L., Bary, J.S. & McGregor, P.J., 2010, *ApJ* 722, 1360
- Bloom, J.S., Starr, D.L., Blake, C.H., Skrutskie, M.F., & Falco, E.E. 2006, in *Astronomical Society of the Pacific Conference Series*, Vol. 351, ed. C.Gabriel, C.Arsviet, D.Ponz & S.Enrique, 751
- Breger, M., Gehrz, R.D., & Hackwell, J.A. 1981, *ApJ*, 248, 963
- Briceño, C., et al. 2004, *ApJ*, 606, L123
- Calvet, N., Hartmann, L., & Strom, S.E. 2000, *Protostars and Planets IV* - University of Arizona Press; eds V.Mannings, A.P.Boss, S.S Russell, p.377
- Calvet, N., & Gullbring, E. 1998, *ApJ*, 509, 802
- Cardelli, J.A., Clayton, G.C. & Mathis, J.S. 1989, *ApJ*, 345, 245
- Caratti o Garatti, A. et al. 2011, *A&A*, 526, L1
- Cohen, M., & Kuhl, L. 1979, *ApJS*, 41, 743
- Cohen, M., Kuhl, L.V., Harlan, E.A., & Spinrad, H. 1981, *ApJ*, 245, 920
- Covey, K.R. et al. 2011, *AJ*, 141, 40

- Cutri, R. M., et al. 2003, Explanatory Supplement to the 2MASS All Sky Data Release(Pasadena: Caltech)
- D’Angelo, C.R., & Spruit, H.C. 2010 MNRAS 406, 1208
- Davis, C.J. et al. 2011, A&A, 528, A3
- Eislöffel, J., Eike, G., Hessman, F.V., Mundt, R., Poetzen, R., Carr, J.S., Beckwith, S., & Ray, T.P. 1991, ApJ, 383, L19
- Fernie, J.D. 1983 PASP 95, 782
- Fischer, W., Edwards, S., Hillenbrand, L., & Kwan, J. 2011 ApJ 730-73
- Gail, H.-P., & Sedlmayr, E. 1999 A&A 347, 594
- Giannini, T. et al. 2009, ApJ, 704, 606
- Giovanardi, C., Gennari, S., Natta, A., & Stanga, R. 1991 ApJ 367, 173
- Gómez, M., & Mardones, D. 2003 AJ 125, 2134
- Gras-Velázquez, A., & Ray, T.P. 2005, A&A, 443, 541
- Guieu, S. et al. 2009 ApJ 697, 787
- Gullbring, E., Hartmann, L., Bričeno, C., & Calvet, N. 1998, ApJ, 492, 323
- Hartigan, P., Edwards, S., & Ghandour, L. 1995, ApJ, 452, 736
- Hartmann, L., & Kenyon, S. 1985, ApJ, 299, 462
- Herbig, G.H. 1989, Proc. of the ESO Workshop on *Low Mass Star Formation and Pre-Main Sequence Objects*, ed. B. Reipurth, p.233
- Herbig, G.H. 1990, ApJ, 360, 639
- Herbig, G.H. 2008, AJ, 135, 637
- Herbig, G.H., Aspin, C., Gilmore, A.C., Imhoff, C.L., Jones, A.F. 2001, PASP, 113, 1547
- Herbig, G.H., & Bell, K.R. 1988, Lick Obs. Bulletin No.1111
- Herbst, W., Herbst, D.K., Grossman, E.J., & Weinstein, D. 1994, AJ, 108, 1906
- Juhász, A. et al. 2011, arXiv: 1110, 3754

- Kazarovets, E.V., Reipurth, B., & Samus, N.N. 2011, *Variablen Stars*, 31, vol.2
- Kenyon, S.J. et al. 1994, *AJ*, 107, 2153
- Kóspál, Á., Ábrahám, P., Prusti, T., Acosta-Pulido, J., Hony, S., Moór, A., & Siebenmorgen, R. 2007, *A&A*, 470, 211
- Kóspál, Á. et al. 2005, *IBVS*, 5661
- Kóspál, Á. et al. 2011, *A&A*, 527, A133
- Kun, M. et al. 2011a, *MNRAS*, 413, 2689
- Kun, M. et al. 2011b, *ApJL*, 733, L8
- Leoni, R., Larionov, V.M., Centrone, M., Giannini, T., & Lorenzetti, D. 2010 *Astronomer's Telegram #2854*
- Liseau, R., Lorenzetti, D., & Molinari, S. 1992, *A&A*, 253, 119
- Lorenzetti, D. et al. 2006, *A&A*, 453, 579
- Lorenzetti, D. et al. 2011b, *ApJ*, 723:69
- Lorenzetti, D., Giannini, T., Larionov, V.M., Kopatskaya, E., Arkharov, A.A., De Luca, M., & Di Paola, A. 2007, *ApJ*, 665, 1193
- Lorenzetti, D., Larionov, V.M., Giannini, T., Arkharov, A.A., Antonucci, S., Nisini, B., & Di Paola, A. 2009, *ApJ*, 693, 1056
- McGehee, P.M. et al. 2004, *ApJ*, 616, 1058
- Menten, K.M., Reid, M.J., Forbrich, J., & Brunthaler, A. 2007, *A&A*, 474, 515
- Meyer, M.R., Calvet, N. & Hillenbrand, L.A. 1997, *AJ*, 114, 288
- Miller, A.A. et al. 2011, *ApJ*, 730, 80
- Muzerolle, J., Calvet, N., Hartmann, L., & D'Alessio, P. 2003, *ApJ*, 597, 149
- Muzerolle, J., D'Alessio, P., Calvet, N., & Hartmann, L. 2004, *ApJ*, 617, 406
- Muzerolle, J., Megeath, S.T., Flaherty, K.M., Gordon, K.D., Rieke, G.H., Young, E.T., & Lada, C.J. 2005, *ApJ*, 620, L107
- Muzerolle, J., Hartmann, L., & Calvet, N. 1998, *AJ*, 116, 2965

- Meyer, M.R., Calvet, N. & Hillenbrand, L.A. 1997, AJ, 114, 288
- Persi, P., Tapia, M., Gòmez, M., Whitney, B.A., Marenzi, A.M., & Roth, M. 2007, AJ, 133, 1690
- Reipurth, B., & Aspin, C. 2004, ApJ 606, L119
- Rieke, G.H. & Lebofsky, M.J. 1985, ApJ, 288, 618
- Semkov, E., & Peneva, S. 2010, Astronomer's Telegram #2801
- Sharp, C.M., & Huebner, W.F. 1990, ApJ, 72, 417
- Sicilia-Aguilar, A. et al. 2008, ApJ, 673, 382
- Shu, F.H., Najita, J.R., Ostriker, E., Wilkin, F., Ruden, S., & Lizano, S. 1994, ApJ, 429, 781
- Sipos, N. et al. 2009, A&A, 507, 881S
- Stecklum, B., Melnikov, S.Y., & Meusinger, H. 2007, A&A, 175, 231
- Straizys, V., Cernis, K., Kazlauskas, A., & Meistas, E. 1992 Balt.Astr., 1, 149
- Takami, M. et al. 2006, ApJ, 641, 357
- Van Citters Jr., G.W., & Smith, S. 1989, AJ, 98, 1328
- Walter, F.M., Stringfellow, G.S., Sherry, W.H., & Field-Pollatou, A. 2004, AJ, 128, 1872
- Xiao, L., Kroll, P., & Henden, A.A. 2010, AJ, 139, 1527

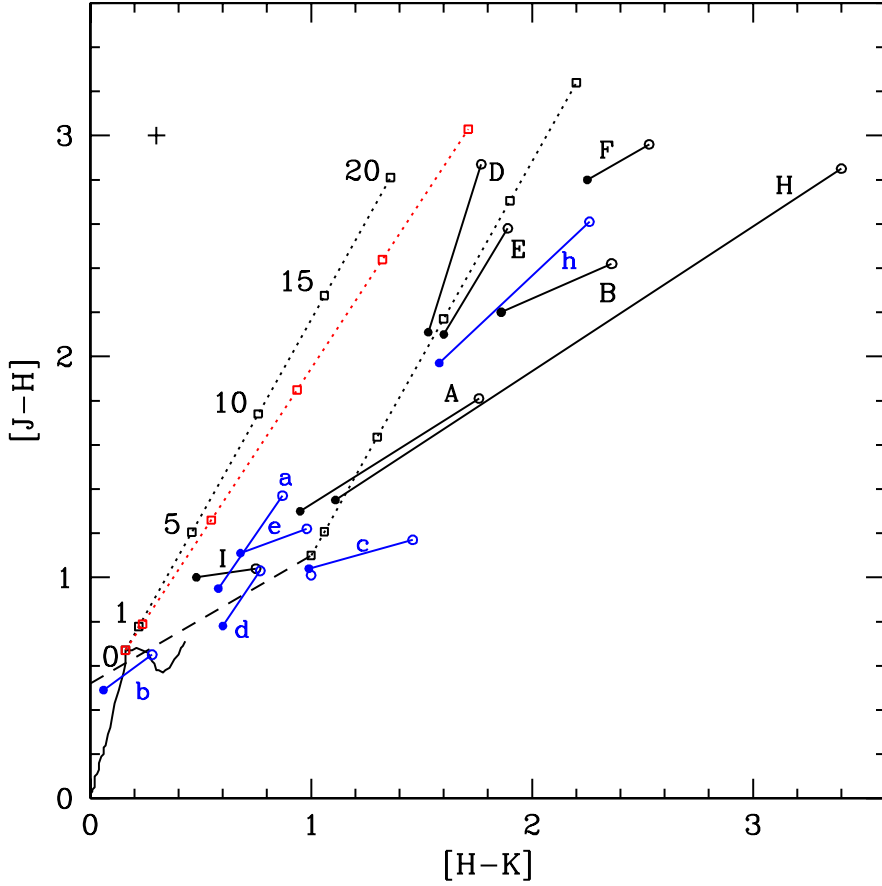


Fig. 1.— Near-IR two-colors diagram of EXor in different epochs. The solid line marks the unreddened main sequence, whereas the dashed one is the locus of the T Tauri stars (Meyer et al. 1997). The black and red dotted lines represent the reddening law by Rieke & Lebofsky (1985) and Cardelli et al. (1989), respectively, where different values of  $A_V$  are indicated by open squares. Sources are alphabetically coded as in Table 1. Solid (open) black circles identify the new targets during their outburst (quiescent) phase. The same is true for the classical EXor stars depicted in blue. These latter evidently overlap much better with the typical locus of T Tauri stars. A cross in the upper left corner indicates the typical error.

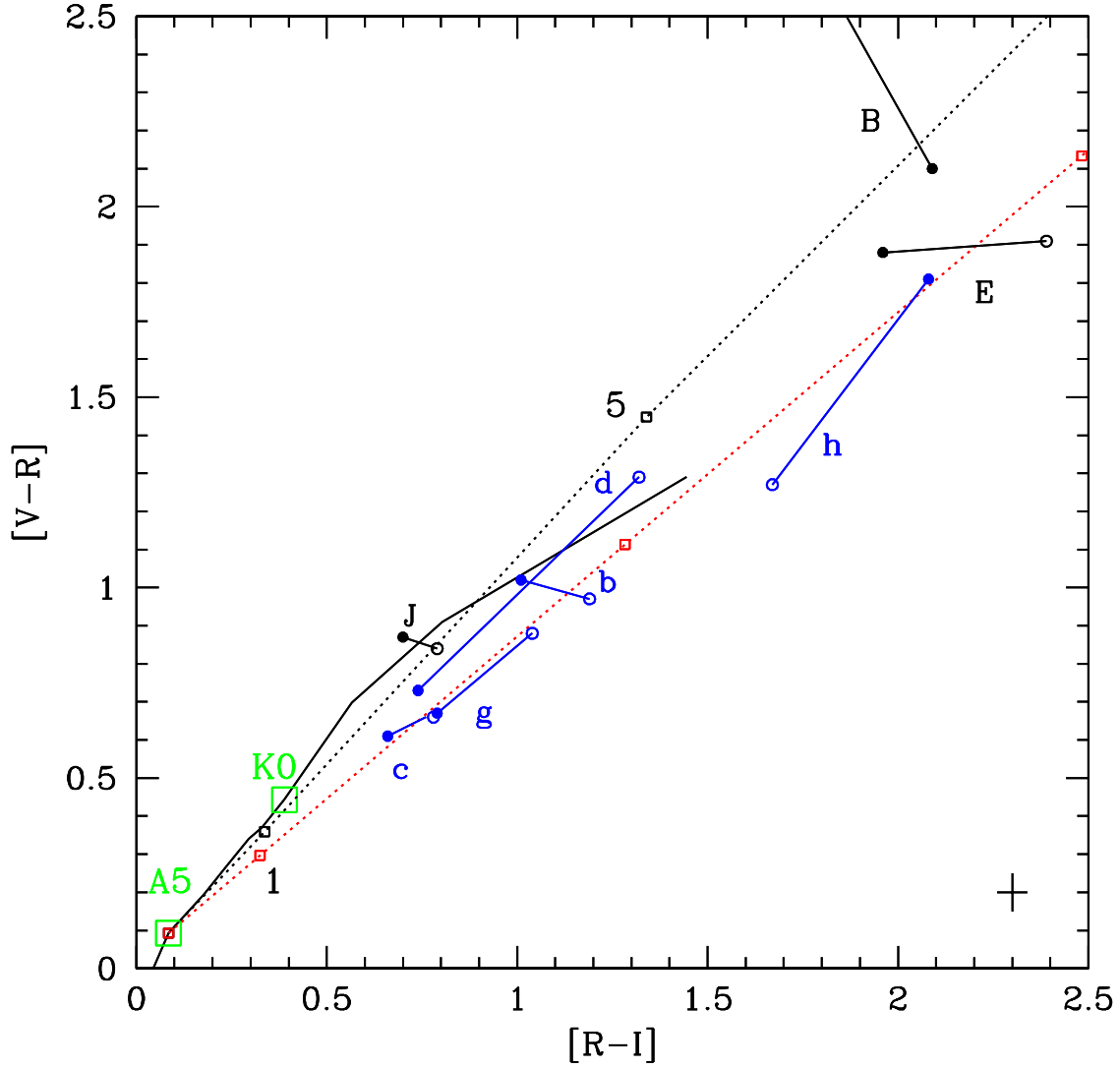


Fig. 2.— Visual two colors diagram of EXor in different epochs. The solid line marks the unreddened main sequence star of a given spectral type as defined by Kenyon & Hartmann (1995) and corrected from Johnson to Cousins system (Ferne 1983); the relevant (see text) spectral types A5 and K0 are indicated as green open squares. The black and red dotted lines represent the reddening law by Rieke & Lebofsky (1985) and Cardelli et al. (1989), respectively, where different values of  $A_V$  are indicated by open squares. Sources are alphabetically coded as in Table 1. Solid (open) black circles identify the new targets during their outburst (quiescent) phase. The same is true for the classical EXor stars depicted in blue. Finally, a cross in the lower right corner indicates the typical error.

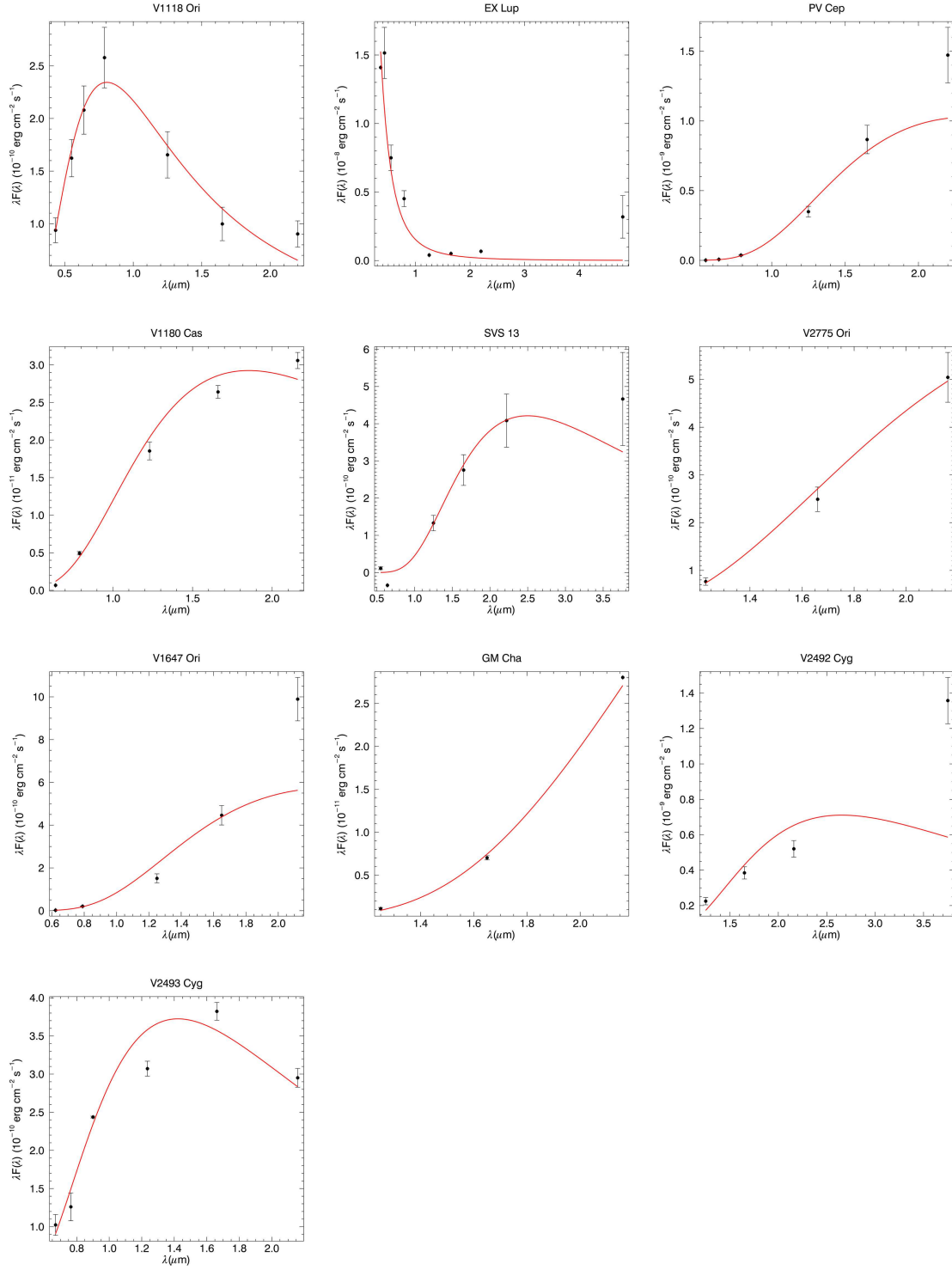


Fig. 3.— Best fits to the SED difference for both classical and newest EXOr. Each curve represents a single temperature BB, whose value is given in Table 4.

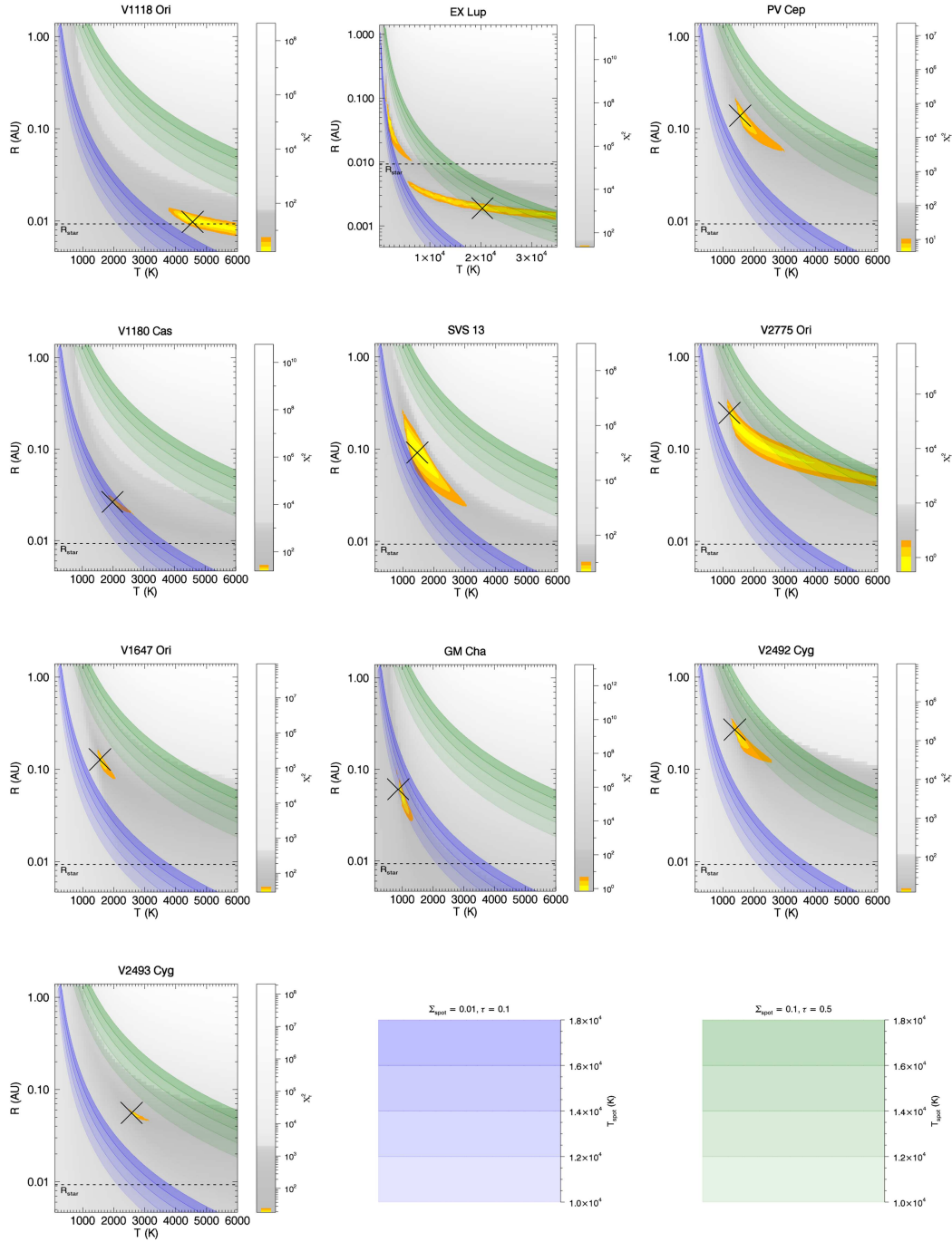


Fig. 4.—  $\chi^2$  maps (grey-scale) projected on the  $(T, R)$  parameters plane with superposed  $1\sigma$  to  $3\sigma$  confidence contours (in yellow and orange, respectively). The dashed horizontal line indicates the stellar radius (assumed  $2 R_{\odot}$ ), while the shaded stripes show the parameters region allowed by the spot model and the energy conservation in a range of spot temperatures  $T_{spot}$  (10000 K to 18000 K) for two values ( $10^{-3}$  and  $5 \cdot 10^{-2}$  in blue and green, respectively) of the  $\tau \cdot \Sigma_{spot}$  product (see text). The color bars relative to these two values, for different spot temperatures, are given in the two bottom panels. The black crosses indicate the pair  $(R, T)$  corresponding to the absolute minimum of  $\chi^2$ .

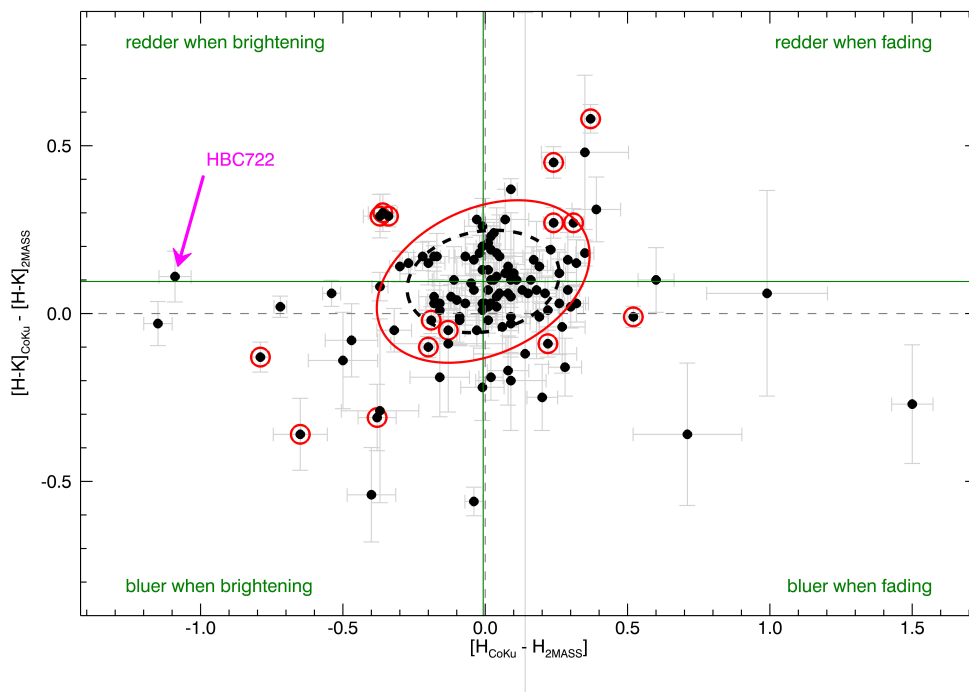


Fig. 5.— Distribution of the color  $[H-K]$  variations vs. the H magnitude variations between early near-IR observations (Cohen & Kuhi 1979) and 2MASS photometry (Cutri et al. 2003) of a sample of low mass YSO’s (mainly CTTSs, see Sect.2). All the sources are depicted with their uncertainty. Among them, circled dots identify sources that (simultaneously) present both magnitude and color variation at a S/N level  $> 5$  and  $> 2.5$ , respectively. Different quadrants are associated with different modalities of variation, shortly indicated in each corner (see also text). The continuous (dashed) ellipse represents  $1\sigma$  of the distribution of the plain (circled) dots. The nominal cartesian vertical and horizontal axes are indicated as dashed lines, but the real ones (solid axes) have been determined using the data points barycenter (see text).

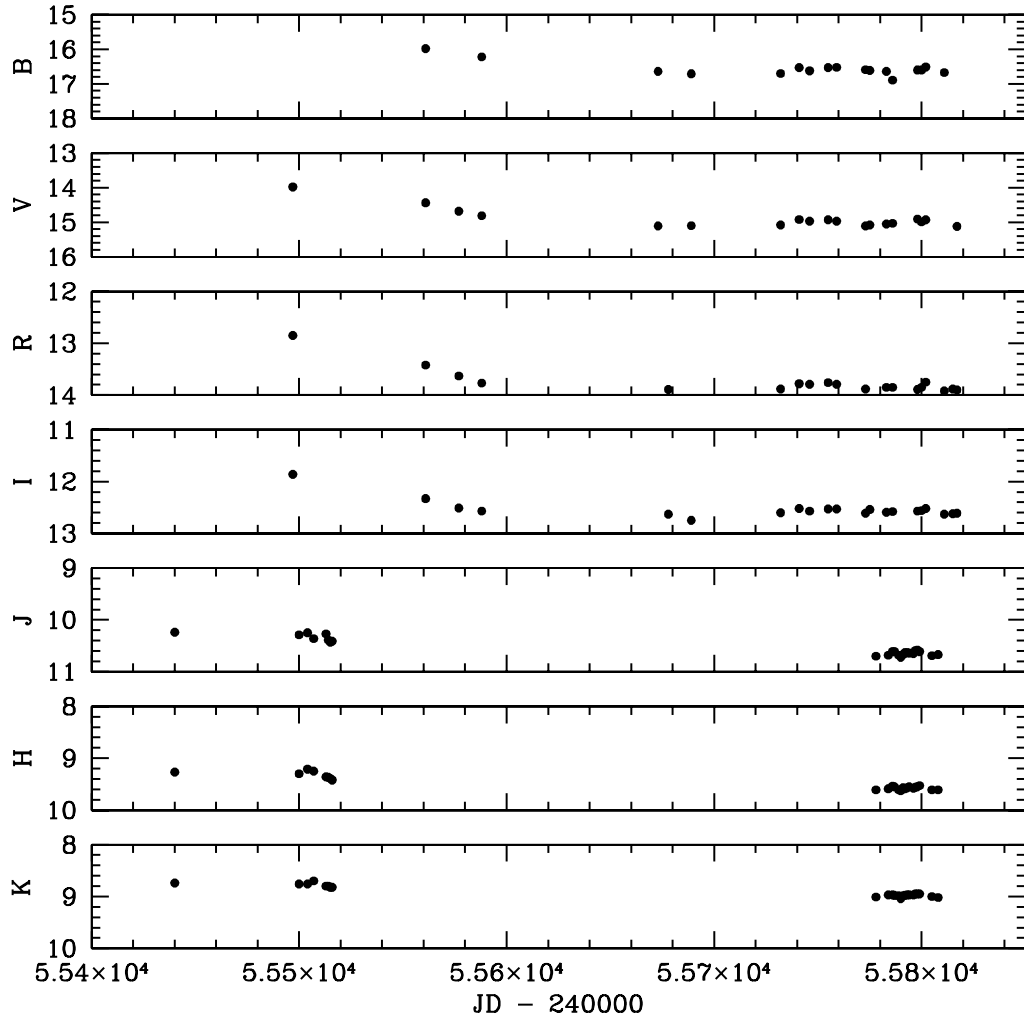


Fig. 6.— V2493 Cyg optical and near-IR light curves vs. Julian Date. The errors of data points are comparable to or less than 0.04 mag.

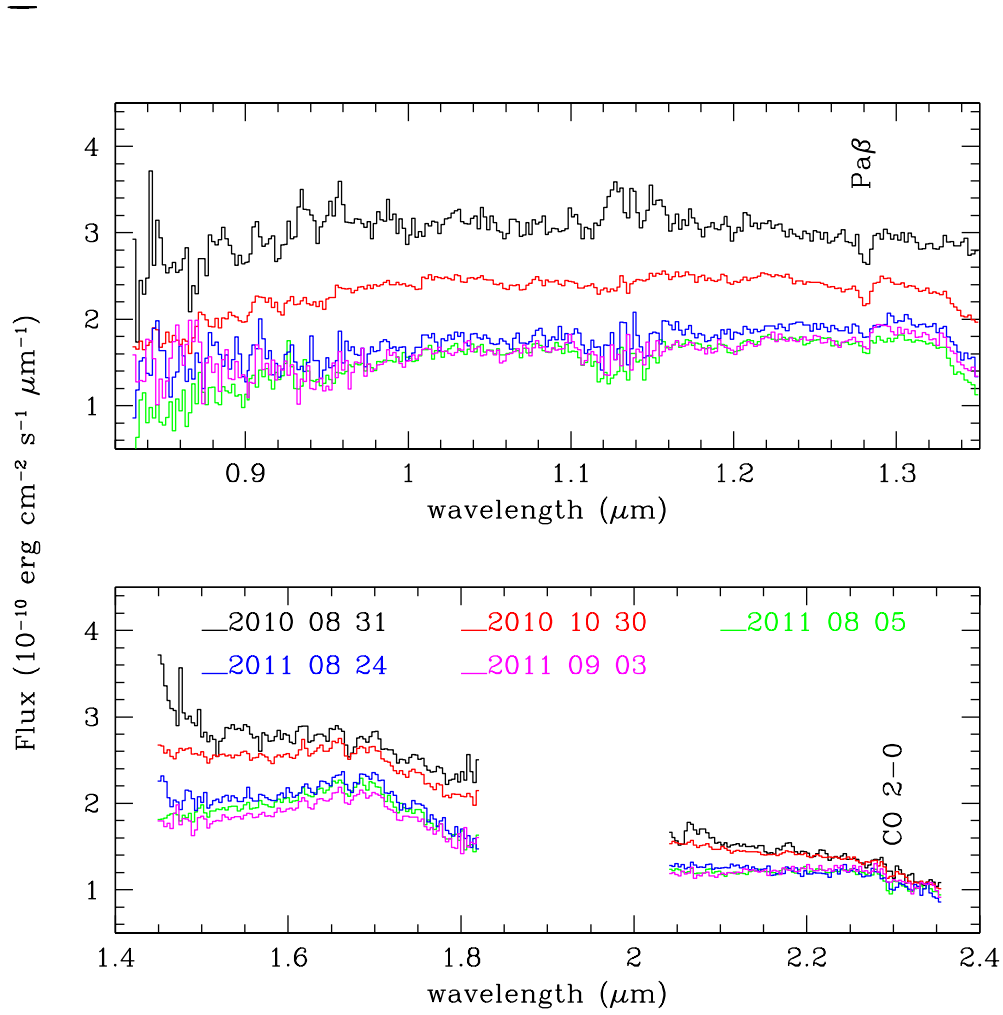


Fig. 7.— Near-IR spectrum of V2493 Cyg obtained on different dates. Detected features are identified.

Table 1. EXor (classical and new detections) relevant observed parameters.

Source	Id. <sup>a</sup>	Distance (pc)	Location	A <sub>V</sub> (mag)	L <sub>bol</sub> (L <sub>⊙</sub> )	V <sub>max</sub> (mag)	V <sub>min</sub> (mag)	References
UZ Tau E	a	140	B19	1.49	1.7 <sup>b</sup>	11.7	15.0	1,2
VY Tau	b	140	L1536	0.85	0.75 <sup>b</sup>	9.0	15.3	1,2,3
DR Tau	c	140	L1558	1.7-2.1	1.05-5.0	10.5	16.0	1,2,4,5
V1118 Ori	d	414	ONC	0-2	1.4-25.4	12.8	17.5	1,6,7
NY Ori	e	414	ONC	0.3	...	14.5	17.5	1,6,8
V1143 Ori	f	500	L1640	...	...	13	19	1
EX Lup	g	140	Lup3	0	0.73	8.4	13.2	1,9,10,11
PV Cep	h	325	L1158	5-7	100	14.6	18.0	12,13,14,15,16
V1180 Cas	A	600	L1340	4.3	0.07	15.7 <sup>e</sup>	> 21	17
SVS13	B	300	NGC1333	6-15	...	15.9 <sup>e</sup>	19.0	18,19,20
LDN1415-IRS	C	170	LDN1415	...	...	14.74 <sup>e</sup>	18.37	21
V2775 Ori	D	450	L1641	18	1.9-22	11.77 <sup>f</sup>	16.4	22
V1647 Ori	E	400	L1630	9-19	5.2 <sup>b</sup>	14.40 <sup>e</sup>	20.27	23,24
					2.8-7.7 <sup>c</sup>			24
					44 <sup>d</sup>			25
GM Cha	F	160	Cha I	13	1.5	10.61 <sup>g</sup>	12.75	26
OO Ser	G	311	Ser NW	42	4.5-(26/36)	11.4 <sup>g</sup>	16.1	27
V2492 Cyg	H	600	IC5070	6-12	20	14.7 <sup>h</sup>	18-19	28,29,30
V2493 Cyg	I	600	NGC7000/IC5070	3.4	2.7-12	13.62	17.0	4
GM Cep	J	900	Tr 37	2-4	30/40	12.43 <sup>h</sup>	14.58	31

<sup>a</sup>Individual sources are identified with the same alphabetical letter used in the colors plots

<sup>b</sup> photospheric luminosity

<sup>c</sup> low state accretion luminosity

<sup>d</sup> outburst bolometric luminosity

<sup>e</sup> I band

<sup>f</sup> J band

<sup>g</sup> K band

<sup>h</sup> R band

Note. — References to the Table: (1) SIMBAD Astronomical Database (<http://simbad.u-strasbg.fr/simbad>); (2) Herbig & Bell 1988; (3) Herbig 1990; (4) Cohen & Kuhi 1979; (5) Kenyon et al. 1994; (6) Menten et al. 2007;

(7) Audard et al. 2010; (8) Breger, Gherz & Hackwell 1981; (9) Gras-Velázquez & Ray 2005; (10) Herbig et al. 2001; (11) Sipos et al. 2009; (12) Cohen et al. 1981; (13) Van Citters & Smith 1989; (14) Lorenzetti et al. 2011; (15) Straizys et al. 1992; (16) Kun et al. 2011a (17) Kun et al. 2011b; (18) Takami et al. 2006; (19) Liseau et al. 1992; (20) Eislöffel et al. 1991; (21) Stecklum et al. 2007; (22) Caratti o Garatti et al. 2011; (23) Briceño et al. 2004; (24) Aspin et al. 2008; (25) Muzerolle et al. 2005; (26) Persi et al. 2007; (27) Kóspál et al. 2007; (28) Covey et al. 2011; (29) Aspin 2011; (30) Kóspál et al. 2011; (31) Sicilia-Aguilar et al. 2008;

Table 2. EXor mass accretion rates in different phases.

Source	Status <sup>a</sup>	$\dot{M}_{acc}$ ( $10^{-7} M_{\odot} \text{ yr}^{-1}$ )	Ref	Method
UZ Tau E	I	1-3	1	Pa $\beta$
DR Tau	I	4-9	1	Pa $\beta$ , Br $\gamma$
V1118 Ori	H	$10 \pm 5$	2	SED modeling
	L	2.5	2	SED modeling
EX Lup	H	$2 \pm 0.5$	3	Br $\gamma$
	L	$0.06 \pm 0.03$	3	Pa $\beta$
PV Cep	H	24	1	Pa $\beta$ , Br $\gamma$
	I	19	1	Pa $\beta$ , Br $\gamma$
V1180 Cas	H	$> 1.6$	4	CaII $\lambda$ 8542
	L	$> 0.16$	4	estimated by Lum. scaling
V1647 Ori	H	$10 \pm 5$	5	Near-IR lines,
	H/I	5.0	6	Near-IR lines,
	L	0.55	6	Near-IR lines,
V2492 Cyg	H	6.4-18	7	Br $\gamma$
	H	2.5	8	Near-IR lines
V2493 Cyg	H	10	9	estimated by Lum. scaling
	L	0.5	10	estimated by the given parameters

<sup>a</sup>H = high; I = intermediate; L = low

Note. — References to the Table: Lorenzetti et al. 2009; (2) Audard et al. 2010; (3) Aspin et al. 2010; (4) Kun et al. 2011; (5) Muzerolle et al. 2005; (6) Acosta-Pulido et al. (2007); (7) Aspin 2011; (8) Covey et al. 2011; (9) Kóspál et al. 2011; (10) Cohen & Kuhl 1979.

Table 3. Fluxes in high and low state.

Source	O/Q <sup>a</sup>	$\lambda \cdot F_{\lambda}$ (erg s <sup>-1</sup> cm <sup>-2</sup> )							Ref.
		B <sup>b</sup>	V	R	I	J	H	K	
V1118 Ori	+	9.09(-11)	1.47(-10)	1.99(-10)	2.62(-10)	2.19(-10)	1.72(-10)	1.29(-10)	1,2
	-	1.35(-12)	2.15(-12)	4.87(-12)	1.10(-11)	3.99(-11)	5.74(-11)	3.42(-11)	1,2
EX Lup <sup>c</sup>	+	2.22(-9)	2.28(-10)	—	2.86(-9)	9.59(-10)	9.61(-10)	9.13(-10)	3
	-	5.63(-11)	1.11(-10)	—	3.43(-10)	4.84(-10)	4.74(-10)	2.82(-10)	4
PV Cep	+	—	2.66(-12)	9.71(-12)	4.42(-11)	3.69(-10)	1.00(-9)	2.04(-9)	5
	-	—	1.14(-12)	2.53(-12)	7.90(-12)	3.01(-11)	1.48(-10)	5.63(-10)	5
V1180 Cas	+	—	—	3.52(-12)	6.33(-12)	2.06(-11)	3.04(-11)	3.97(-11)	6
	-	—	—	1.51(-13)	2.12(-13)	9.81(-13)	2.48(-12)	6.58(-12)	6,7
SVS 13 <sup>d</sup>	+	—	1.71(-13)	8.15(-13)	—	5.58(-11)	1.88(-10)	4.95(-10)	8,9
	-	—	6.31(-15)	1.09(-13)	—	1.11(-11)	4.60(-11)	1.92(-10)	8,9
V2775 Ori	+	—	—	—	—	7.58(-11)	2.53(-10)	5.18(-10)	10
	-	—	—	—	—	1.07(-12)	7.15(-12)	1.83(-11)	10
V1647 Ori	+	—	—	1.92(-12)	1.68(-11)	1.50(-10)	4.64(-10)	1.06(-9)	11,12,13
	-	—	4.21(-15)	1.22(-14)	7.54(-14)	5.09(-12)	2.43(-11)	7.56(-11)	7,11,14,15,16
GM Cha	+	—	—	—	—	1.54(-12)	9.09(-12)	3.79(-11)	7
	-	—	—	—	—	2.09(-13)	1.43(-12)	7.70(-12)	17
V2492 Cyg <sup>e</sup>	+	—	—	—	—	2.25(-10)	3.85(-10)	5.28(-10)	18
	-	—	—	—	—	7.31(-14)	4.51(-13)	5.18(-12)	19
V2493 Cyg <sup>f</sup>	+	—	—	1.33(-10)	1.86(-10)	3.49(-10)	4.19(-10)	3.27(-10)	20
	-	—	—	2.41(-12)	7.62(-12)	1.94(-11)	2.41(-11)	2.41(-11)	7,21

<sup>a</sup>+ = high state; - = low state

<sup>b</sup>photometric bands are conventionally associated (see text) to the following effective wavelengths (in  $\mu\text{m}$ ): B 0.43, V 0.55, R 0.64, I 0.79, J 1.25, H 1.65, K 2.20

<sup>c</sup>Fluxes are also obtained at U (0.36 $\mu\text{m}$ ): 1.32(-9)/3.08(-11); M (4.80 $\mu\text{m}$ ): 3.20(-9)/1.10(-10).

<sup>d</sup>Fluxes are also obtained at L' (3.76 $\mu\text{m}$ ): 1.56(-9)/1.06(-9).

<sup>e</sup>Fluxes are also obtained at L' (3.75 $\mu\text{m}$ ): 1.43(-9)/6.16(-11).

<sup>f</sup>Fluxes are also obtained at z' (0.90 $\mu\text{m}$ ): 2.65(-10)/6.06(-12).

Note. — References to the Table: (1) Audard et al. 2010; (2) Lorenzetti et al. 2006; (3) Aspin et al. 2010; (4) Sipos et al. 2009; (5) Lorenzetti et al. 2011; (6) Kun et al. 2011b; (7) Cutri et al. 2003 (2MASS); (8) Liseau et al. 1992; (9) Eislöffel et al. 1991; (10) Caratti o Garatti et al. 2011; (11) Briceño et al. 2004; (12) Reipurth & Aspin 2004; (13) Andrews et al. 2004; (14) Kóspál et al. 2005; (15) Aspin & Reipurth 2009; (16) Ábrahám et al. 2004; (17) Persi et al.

2007; (18) Covey et al. 2011; (19) Aspin 2011; (20) Miller et al. 2011; (21) Guieu et al. 2009.

Table 4. Ranges of the fit parameters corresponding to the best  $\chi^2$  values compatible with the spot model (blue and green regions in Figure 4).

Source	$\chi^2$	T (K)	R (AU)	$A_V^{quiesc}$ (mag)	$\Delta A_V$ (mag)
V1118Ori	1.64	$4546^{+1454}_{-460}$	$0.01^{+0.00}_{-0.00}$	$2.1^{+2.0}_{-2.1}$	$-1.9^{+2.4}_{-0.7}$
EXLup	21.7	$20332^{+14668}_{-19242}$	$0.002^{+0.12}_{-0.00}$	$3.1^{+11.9}_{-0.9}$	$-1.5^{+0.4}_{-1.4}$
PVCep	4.37	$1554^{+211}_{-82}$	$0.14^{+0.02}_{-0.02}$	$0.9^{+1.8}_{-0.6}$	$-0.7^{+0.4}_{-0.3}$
V1180 Cas	15.54	$1981^{+67}_{-98}$	$0.03^{+0.00}_{-0.00}$	$4.3^{+0.9}_{-0.4}$	$-4.2^{+0.3}_{-0.7}$
SVS13	4.60	$1468^{+685}_{-407}$	$0.09^{+0.08}_{-0.04}$	$9.8^{+5.2}_{-6.5}$	$-3.4^{+0.3}_{-0.1}$
V2775 Ori	0.30	$1212^{+3162}_{-46}$	$0.25^{+0.02}_{-0.18}$	$0.0^{+15}_{-0.0}$	$-0.1^{+4.9}_{-5.1}$
V1647Ori	29.06	$1554^{+82}_{-61}$	$0.13^{+0.01}_{-0.01}$	$5.5^{+0.2}_{-3.4}$	$-5.0^{+3.0}_{-0.0}$
GM Cha	0.70	$870^{+227}_{-22}$	$0.06^{+0.01}_{-0.02}$	$5.8^{+8.8}_{-2.7}$	$-5.0^{+1.9}_{-0.0}$
V2492Cyg	12.6	$1383^{+178}_{-70}$	$0.27^{+0.01}_{-0.06}$	$4.6^{+2.2}_{-4.6}$	$-4.6^{+4.6}_{-0.4}$
V2493 Cyg	18.07	$2580^{+183}_{-17}$	$0.06^{+0.00}_{-0.01}$	$4.3^{+0.3}_{-4.3}$	$-4.2^{+4.5}_{-0.2}$

Table 5. Optical and near-IR photometry of V2493 Cyg.

Date JD-2400000	B	V	R	I (mag)	J	H	K
43449 <sup>a</sup>	—	—	—	—	—	11.12	10.26
51705 <sup>b</sup>	—	—	—	—	13.25	12.21	11.46
55440 <sup>c</sup>	—	—	—	—	10.24	9.27	8.74
55497	—	13.98	12.85	11.86	—	—	—
55500 <sup>c</sup>	—	—	—	—	10.29	9.30	8.76
55504	—	—	—	—	10.25	9.21	8.76
55507	—	—	—	—	10.36	9.25	8.70
55513	—	—	—	—	10.27	9.36	8.80
55514	—	—	—	—	10.39	9.37	8.80
55515	—	—	—	—	10.43	9.39	8.82
55516	—	—	—	—	10.41	9.42	8.82
55561	15.98	14.44	13.42	12.33	—	—	—
55577	—	14.68	13.63	12.51	—	—	—
55588	16.22	14.81	13.77	12.57	—	—	—
55673	16.64	15.11	—	—	—	—	—
55678	—	—	13.89	12.63	—	—	—
55689	16.71	15.10	—	12.75	—	—	—
55732	16.70	15.08	13.88	12.60	—	—	—
55741	16.53	14.92	13.78	12.52	—	—	—
55746	16.62	14.97	13.79	12.57	—	—	—
55755	16.53	14.93	13.76	12.53	—	—	—
55759	16.52	14.97	13.79	12.53	—	—	—
55773	16.59	15.11	13.88	12.61	—	—	—
55775	16.61	15.08	—	12.54	—	—	—
55778 <sup>c</sup>	—	—	—	—	10.70	9.61	9.01
55783	16.64	15.05	13.85	12.59	—	—	—
55784	—	—	—	—	10.68	9.59	8.97
55786	16.89	15.03	13.85	12.58	10.61	9.54	8.97
55787	—	—	—	—	10.61	9.55	8.98
55789	—	—	—	—	10.68	9.61	8.99
55790	—	—	—	—	10.72	9.63	9.04
55791	—	—	—	—	10.67	9.57	8.99
55792	—	—	—	—	10.63	9.59	8.98
55793	—	—	—	—	10.63	9.57	8.97
55794	—	—	—	—	10.64	9.55	8.97

Table 5—Continued

Date JD-2400000	B	V	R	I (mag)	J	H	K
55796	—	—	—	—	10.65	9.58	8.97
55797 <sup>c</sup>	—	—	—	—	10.59	9.56	8.95
55798	16.60	14.91	13.89	12.57	10.58	9.55	8.95
55799	—	—	—	—	10.61	9.53	8.95
55800	16.60	14.99	13.85	12.56	—	—	—
55802	16.51	14.93	13.75	12.52	—	—	—
55805	—	—	—	—	10.69	9.61	9.00
55808 <sup>c</sup>	—	—	—	—	10.67	9.61	9.02
55811	16.67	—	13.92	12.63	—	—	—
55815	—	—	13.88	12.62	—	—	—
55817	—	15.12	13.90	12.61	—	—	—

<sup>a</sup>Early observation (1977) by CoKu.

<sup>b</sup>2MASS observation (2000).

<sup>c</sup>Date on which a near-IR spectrum has been taken (see Figure 7).

Note. — Typical errors of the optical/near-IR magnitude are less than 0.04 mag.